



Central schemes on overlapping cells

Yingjie Liu

School of Mathematics, Georgia Institute of Technology, Atlanta, GA 30332, United States

Received 21 June 2004; received in revised form 4 January 2005; accepted 14 March 2005

Available online 5 May 2005

Dedicated to James Glimm on the occasion of his 70th birthday

Abstract

Nessyahu and Tadmor's central scheme [J. Comput. Phys. 87 (1990)] has the benefit of not using Riemann solvers for solving hyperbolic conservation laws. But the staggered averaging causes large dissipation when the time step size is small compared to the mesh size. The recent work of Kurganov and Tadmor [J. Comput. Phys. 160 (2000)] overcomes this problem by using a variable control volume and results in semi-discrete and fully discrete non-staggered schemes. Motivated by this work, we introduce overlapping cell averages of the solution at the same discrete time level, and develop a simple alternative technique to control the $O(1/\Delta t)$ dependence of the dissipation. The semi-discrete form of the central scheme can also be obtained to which the TVD Runge–Kutta time discretization methods of Shu and Osher [J. Comput. Phys. 77 (1988)] or other stable and sufficiently accurate ODE solvers can be applied. This technique is essentially independent of the reconstruction and the shape of the mesh. The overlapping cell representation of the solution also opens new possibilities for reconstructions. Generally speaking, more compact reconstruction can be achieved. In the following, schemes of up to fifth order in 1D and third order in 2D have been developed. We demonstrate through numerical examples that by combining two classes of the overlapping cells in the reconstruction we can achieve higher resolution.

© 2005 Elsevier Inc. All rights reserved.

MSC: 65M60; 65M12

Keywords: Central scheme; ENO scheme; MUSCL scheme; TVD scheme

1. Introduction

The central scheme of Nessyahu and Tadmor (NT) uses a staggered grid to avoid solving Riemann problems at cell edges and provides a black box solution to nonlinear hyperbolic conservation laws. In [31], a

E-mail address: yingjie@math.gatech.edu.

third order non-oscillatory central scheme was developed. In [6], third and fourth order central schemes with ENO [10] reconstruction have been developed, in particular, the natural continuous extension of the Runge–Kutta method [44] has been used in the evaluation of the flux integral which greatly improves the efficiency for higher order central schemes. The recent work of Pareschi et al. [33] on the central Runge–Kutta schemes does not use a quadrature rule in time for the fluxes, which further improves the efficiency. In [25–27], a series of central WENO schemes have been developed with increasing order of accuracy. In [11], a general procedure is introduced to develop central schemes on non-staggered grids. Central schemes typically require the approximation of the flux integrated over time which in turn requires the evaluation of the fluxes at middle time steps. In [1], solutions in previous time levels are used in the prediction of the flux at middle time steps which reduces the computational cost in multi space dimensions. Since central schemes usually use staggered averages, the time step size cannot be passed to zero. Kurganov and Tadmor [18] solve the problem by using a variable control volume whose size depends on the time step size. By passing to the limit as the time step size goes to zero, non-staggered semi-discrete schemes can be developed which also reveal a connection between staggered central schemes and non-staggered schemes with the Lax–Friedrichs flux instead of solving Riemann problems (e.g. ENO-LLF [40]), see also the review article by Shu [38]. Higher order developments can be found, e.g., in [20,16]. Semi-discrete schemes can be used for a larger class of equations where the time step size is sometimes small compared to the mesh size. The TVD Runge–Kutta time discretization methods of Shu and Osher [39] or other stable and sufficiently accurate ODE solvers can be applied to the semi-discrete schemes to obtain fully discrete schemes. Besides central schemes and schemes with the Lax–Friedrichs flux, the relaxation scheme of Jin and Xin [14] also has no need to solve Riemann problems. High order central WENO schemes with or without local characteristic decomposition have been studied by Qiu and Shu [34]. We would like to refer to [5,13,19,7,41] etc. for more related works.

In this paper, we introduce a new technique to control the dissipative error of the staggered central schemes. The major idea is to introduce overlapping cell representation of the solution. An immediate advantage is that the time discretization becomes simple by the use of the TVD Runge–Kutta methods. Also by using a time step size dependent convex combination of the overlapping cell averages, the $O(1/\Delta t)$ dependent dissipative error can be easily controlled. Although the use of overlapping cells generally doubles the computational cost, more efficient reconstruction methods using the combined information from the overlapping cell averages could improve the resolution.

In Section 2, we introduce the 1D formulations of the central schemes on overlapping cells and introduce the technique to control the dissipative error related to the small time step size. In Section 3, we discuss the application to convection–diffusion equations for which the small time step size is usually required for explicit schemes. The reconstruction procedures for 1D overlapping cells are discussed in Section 4. In Section 5, we extend the techniques to 2D. 1D and 2D numerical examples are given in Section 6.

2. Central schemes for scalar conservation laws in one space dimension

Consider the 1D conservation law

$$\begin{aligned} \frac{\partial u}{\partial t} + \frac{\partial f(u)}{\partial x} &= 0, \quad (x, t) \in R \times (0, T), \\ u(x, 0) &= u_0(x), \quad x \in R. \end{aligned} \quad (1)$$

Let $\{x_i\}$ be a uniform partition in R with $\Delta x = x_{i+1} - x_i$ and $x_{i+1/2} = \frac{1}{2}(x_i + x_{i+1})$. Let $U_i(t)$ approximate the cell average $\int_{x_{i-1/2}}^{x_{i+1/2}} u(x, t) dx$ and $U_{i+1/2}(t)$ approximate the cell average $\int_{x_i}^{x_{i+1}} u(x, t) dx$, $U_i^n = U_i(t_n)$, $U_{i+1/2}^n = U_{i+1/2}(t_n)$ (see Fig. 2). By applying a MUSCL [42] or ENO [10] or any other non-oscillatory reconstruction procedure to the two sets of cell averages, one obtains a function $\mu^n(x)$ which is a piecewise

polynomial for cells $\{(x_{i-1/2}, x_{i+1/2}) : i = 0, \pm 1, \pm 2, \dots\}$ and a function $v^n(x)$ which is a piecewise polynomial for cells $\{(x_i, x_{i+1}) : i = 0, \pm 1, \pm 2, \dots\}$. They satisfy $\frac{1}{\Delta x} \int_{x_{i-1/2}}^{x_{i+1/2}} \mu^n(x) dx = U_i^n$ and $\frac{1}{\Delta x} \int_{x_i}^{x_{i+1}} v^n(x) dx = U_{i+1/2}^n$. Let $\Delta t_n = t_{n+1} - t_n$ be the current time step size. The central scheme on overlapping cells can be written in the forward Euler form as follows:

$$\begin{aligned} U_i^{n+1} &= \frac{1}{\Delta x} \int_{x_{i-1/2}}^{x_{i+1/2}} v^n(x) dx - \frac{\Delta t_n}{\Delta x} [f(v^n(x_{i+1/2})) - f(v^n(x_{i-1/2}))], \\ U_{i+1/2}^{n+1} &= \frac{1}{\Delta x} \int_{x_i}^{x_{i+1}} \mu^n(x) dx - \frac{\Delta t_n}{\Delta x} [f(\mu^n(x_{i+1})) - f(\mu^n(x_i))]. \end{aligned} \quad (2)$$

Kurganov and Tadmor [18] point out that since the numerical dissipation from $\frac{1}{\Delta x} \int_{x_{i-1/2}}^{x_{i+1/2}} v^n(x) dx$ does not depend on Δt_n , the cumulative error depends on $O(1/\Delta t)$, the total number of time steps in the computation. Therefore when Δt is very small, e.g. $\Delta t = O(\Delta x^2)$ in some situations, the numerical dissipation becomes large. This is easy to understand if $f(u) \equiv 0$, then what the central scheme does is conservative rezoning at every time step, which will smear out the solution with increasing number of time steps. By choosing the size of the control volume (x_i, x_{i+1}) proportional to Δt as in [18], this $O(1/\Delta t)$ dependence can be removed and by passing to the limit as $\Delta t \rightarrow 0$, semi-discrete schemes can be developed. Here we introduce another technique to remove the $O(1/\Delta t)$ dependence of the error taking advantage of the overlapping cell representations U_i^n and $U_{i+1/2}^n$. The idea is to use a time dependent weighted average of $\frac{1}{\Delta x} \int_{x_{i-1/2}}^{x_{i+1/2}} v^n(x) dx$ and U_i^n in the first equation of (2), which does not change the order of accuracy of the scheme. In fact the difference between them is the local dissipation error. Suppose $\Delta t_n \leq \Delta \tau_n$ and $\Delta \tau_n$ is an upper bound for the current time step size due to the CFL restriction. The forward Euler form of the new central scheme can be formulated as follows:

$$\begin{aligned} U_i^{n+1} &= \theta \left(\frac{1}{\Delta x} \int_{x_{i-1/2}}^{x_{i+1/2}} v^n(x) dx \right) + (1 - \theta) U_i^n - \frac{\Delta t_n}{\Delta x} [f(v^n(x_{i+1/2})) - f(v^n(x_{i-1/2}))], \\ U_{i+1/2}^{n+1} &= \theta \left(\frac{1}{\Delta x} \int_{x_i}^{x_{i+1}} \mu^n(x) dx \right) + (1 - \theta) U_{i+1/2}^n - \frac{\Delta t_n}{\Delta x} [f(\mu^n(x_{i+1})) - f(\mu^n(x_i))], \end{aligned} \quad (3)$$

where $\theta = \Delta t_n / \Delta \tau_n$. See Figs. 1 and 3. Note that when $\theta = 1$, it becomes scheme (2). One can also obtain the following semi-discrete form by moving U_i^n and $U_{i+1/2}^n$ to the left-hand side and multiplying both sides by $\frac{1}{\Delta t_n}$, then passing to the limit as $\Delta t_n \rightarrow 0$,

$$\begin{aligned} \frac{d}{dt} U_i(t_n) &= \frac{1}{\Delta \tau_n} \left[\frac{1}{\Delta x} \int_{x_{i-1/2}}^{x_{i+1/2}} v^n(x) dx - U_i^n \right] - \frac{1}{\Delta x} [f(v^n(x_{i+1/2})) - f(v^n(x_{i-1/2}))], \\ \frac{d}{dt} U_{i+1/2}(t_n) &= \frac{1}{\Delta \tau_n} \left[\frac{1}{\Delta x} \int_{x_i}^{x_{i+1}} \mu^n(x) dx - U_{i+1/2}^n \right] - \frac{1}{\Delta x} [f(\mu^n(x_{i+1})) - f(\mu^n(x_i))]. \end{aligned} \quad (4)$$

The forward Euler forms (2) and (3) are only first order accurate in time, but they can be used as building blocks of the Heun scheme or the high order TVD Runge–Kutta time discretization methods [39]. To study the non-oscillatory property of scheme (3), denote $\text{TV}\{U_i^{n+1}\} = \sum_i |U_{i+1}^{n+1} - U_i^{n+1}|$ as the total variation of U_i^{n+1} . We say scheme (2) or (3) is TVD from the time t_n to t_{n+1} if

$$\max\{\text{TV}\{U_i^{n+1}\}, \text{TV}\{U_{i+1/2}^{n+1}\}\} \leq \max\{\text{TV}\{U_i^n\}, \text{TV}\{U_{i+1/2}^n\}\} < \infty.$$

Theorem 1. *Let schemes (2) and (3) start from the same time t_n with the same initial values U_i^n and $U_{i+1/2}^n$. If scheme (2) is TVD from the time t_n to $t_n + \Delta \tau_n$, then scheme (3) is also TVD from the time t_n to $t_n + \Delta t_n$ for any $\Delta t_n \in [0, \Delta \tau_n]$.*

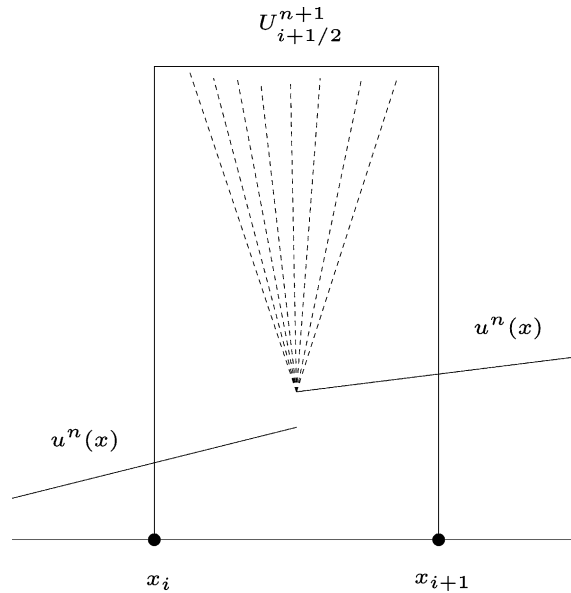


Fig. 1. Nessyahu and Tadmor's central scheme.

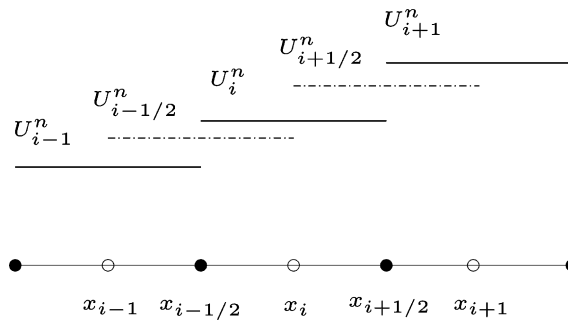


Fig. 2. 1D overlapping cells.

Proof. Note that the first equation of (3) can be rewritten as

$$U_i^{n+1} = \theta \left\{ \frac{1}{\Delta x} \int_{x_{i-1/2}}^{x_{i+1/2}} v^n(x) dx - \frac{\Delta \tau_n}{\Delta x} [f(v^n(x_{i+1/2})) - f(v^n(x_{i-1/2}))] \right\} + (1 - \theta) U_i^n.$$

This is a convex combination of U_i^n and $U_{i+1/2}^{n+1}$ computed by scheme (2) with the time step size $\Delta \tau_n$. Since scheme (2) is TVD for the time step size $\Delta \tau_n$, $U_{i+1/2}^{n+1}$ computed by scheme (3) satisfies

$$\text{TV}\{U_i^{n+1}\} \leq \max\{\text{TV}\{U_i^n\}, \text{TV}\{U_{i+1/2}^{n+1}\}\} < \infty.$$

Similarly from the second equation of (3) we conclude that $U_{i+1/2}^{n+1}$ computed by (3) satisfies

$$\text{TV}\{U_{i+1/2}^{n+1}\} \leq \max\{\text{TV}\{U_i^n\}, \text{TV}\{U_{i+1/2}^n\}\}.$$

The proof is complete. \square

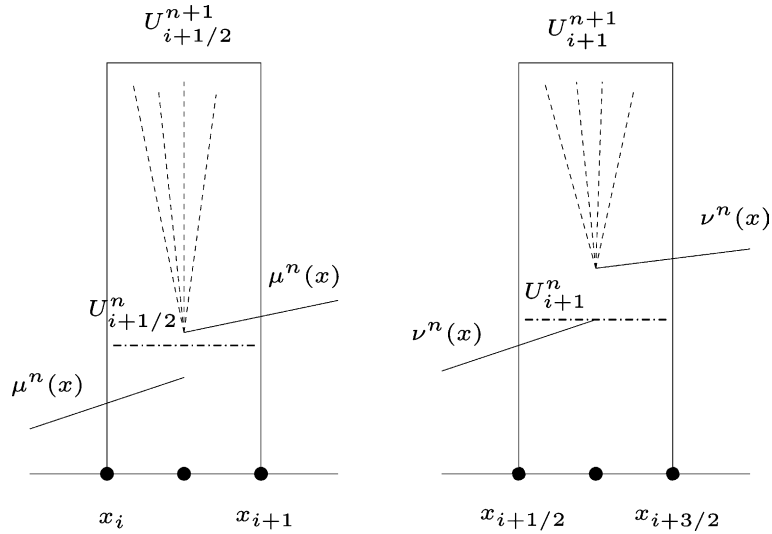


Fig. 3. Central scheme on overlapping cells allows a convex combination of the cell averages.

Remark. The proof follows closely the strategy used in [39]. If we change the definition of the total variation to

$$TV\{U_i^{n+1}\} = \sum_{2i=0,\pm 1,\pm 2,\dots} |U_i^{n+1} - U_{i-1/2}^{n+1}|,$$

Theorem 1 is still true following a similar argument. These two versions of the theorem provide us with some insights into two reconstruction procedures: one is a standard reconstruction from two classes of cell averages $\{U_i^n : i = 0, \pm 1, \pm 2, \dots\}$ and $\{U_{i+1/2}^n : i = 0, \pm 1, \pm 2, \dots\}$ separately; the other mixes the two classes in the reconstruction. We will discuss more about the latter in the following sections.

Note that in (3),

$$\theta \left(\frac{1}{\Delta x} \int_{x_{i-1/2}}^{x_{i+1/2}} v^n(x) dx \right) + (1 - \theta)U_i^n = U_i^n + \frac{\Delta t_n}{\Delta \tau_n} \left(\frac{1}{\Delta x} \int_{x_{i-1/2}}^{x_{i+1/2}} v^n(x) dx - U_i^n \right),$$

$\Delta \tau_n = O(\Delta x)$ is due to the CFL restriction for scheme (2). Therefore the local dissipative error now has a factor Δt_n and the cumulative error will not be degenerated by choosing very small Δt_n . It is interesting to study the lowest order case of (3) and compare it to the Lax–Friedrichs scheme [21],

$$U_i^{n+1} = \theta \frac{U_{i-1/2}^n + U_{i+1/2}^n}{2} + (1 - \theta)U_i^n - \frac{\Delta t_n}{\Delta x} \{f(U_{i+1/2}^n) - f(U_{i-1/2}^n)\} = U_i^n - \frac{\Delta t_n}{\Delta x/2} \{F_{i+1/4}^n - F_{i-1/4}^n\},$$

where $F_{i+1/4}^n = \frac{1}{2} \{f(U_i^n) + f(U_{i+1/2}^n)\} + \frac{1}{2} \frac{\Delta x/2}{\Delta \tau_n} (U_i^n - U_{i+1/2}^n)$. This is the Lax–Friedrichs flux with the diffusive coefficient $\frac{\Delta x/2}{\Delta \tau_n}$ (see, e.g., [38]), which should be chosen to be larger than $\max_u |f'(u)|$ in order for the flux $F_{i+1/4}^n$ to be a monotone flux. Therefore (3) in the lowest order case can be viewed as a finite volume scheme with the Lax–Friedrichs flux. When $\theta = 1$, i.e. $\Delta t_n = \Delta \tau_n$, it becomes the original non-staggered Lax–Friedrichs scheme on a mesh of size $\Delta x/2$.

Remark. 1. The CFL restriction for (2) (thus (3) by Theorem 1) requires that

$$\Delta\tau_n \sup_u |f'(u)|/\Delta x \leq \frac{1}{2},$$

where the left-hand side is called the CFL factor. $\Delta\tau_n$ controls the dissipation (which increases with decreasing $\Delta\tau_n$). Once it is set, the actual time step size Δt_n must be no larger than $\Delta\tau_n$. For the TVD Runge–Kutta methods of orders up to 3, θ can take any value in $[0, 1]$. For purely hyperbolic problems, θ should be chosen as large as possible (i.e., 1) in order to reduce the computational cost. In most of the numerical experiments we only show the results with $\theta = \frac{1}{2}$ for the purpose of testing the schemes, and find no significant difference among the solutions for any $\theta \in (0, 1]$. In one form of the fourth order TVD Runge–Kutta methods [39], its CFL factor (not the CFL factor for choosing $\Delta\tau_n$) is no larger than $2/3$, which implies that $\theta \leq 2/3$ when applying it to the semi-discrete scheme (4).

2. The Glimm scheme [8] is formulated on the staggered grid. By using overlapping cells, it could also be written in a semi-discrete form parallel to the procedure from (2) through (4).

3. Central schemes for convection–diffusion equations in one space dimension

Consider the convection–diffusion equation

$$\begin{aligned} \frac{\partial u}{\partial t} + \frac{\partial f(u)}{\partial x} &= \frac{\partial}{\partial x} \left(a(u, x, t) \frac{\partial u}{\partial x} \right), \quad (x, t) \in R \times (0, T), \\ u(x, 0) &= u_0(x), \quad x \in R, \end{aligned} \tag{5}$$

where $a(u, x, t) \geq 0$. Following the work of Kurganov and Tadmor [18], we can discretize Eq. (5) as follows:

$$\begin{aligned} U_i^{n+1} &= \theta \left(\frac{1}{\Delta x} \int_{x_{i-1/2}}^{x_{i+1/2}} v^n(x) dx \right) + (1 - \theta) U_i^n - \frac{\Delta t_n}{\Delta x} [f(v^n(x_{i+1/2})) - f(v^n(x_{i-1/2}))] \\ &\quad + \frac{\Delta t_n}{\Delta x} \left[a(U_{i+1/2}^n, x_{i+1/2}, t_n) \frac{U_{i+1}^n - U_i^n}{\Delta x} - a(U_{i-1/2}^n, x_{i-1/2}, t_n) \frac{U_i^n - U_{i-1}^n}{\Delta x} \right], \\ U_{i+1/2}^{n+1} &= \theta \left(\frac{1}{\Delta x} \int_{x_i}^{x_{i+1}} \mu^n(x) dx \right) + (1 - \theta) U_{i+1/2}^n - \frac{\Delta t_n}{\Delta x} [f(\mu^n(x_{i+1})) - f(\mu^n(x_i))] \\ &\quad + \frac{\Delta t_n}{\Delta x} \left[a(U_{i+1}^n, x_{i+1}, t_n) \frac{U_{i+3/2}^n - U_{i+1/2}^n}{\Delta x} - a(U_i^n, x_i, t_n) \frac{U_{i+1/2}^n - U_{i-1/2}^n}{\Delta x} \right], \end{aligned} \tag{6}$$

where $\theta = \Delta t_n/\Delta\tau_n$, $\Delta\tau_n$ is the maximum time step size determined by the CFL restriction for the hyperbolic part of Eq. (5), $\frac{\partial u}{\partial t} + \frac{\partial f(u)}{\partial x} = 0$.

Theorem 2. Let schemes (2) and (6) start from the same time t_n with the same initial values U_i^n and $U_{i+1/2}^n$. If scheme (2) is TVD from the time t_n to $t_n + \Delta\tau_n$, then scheme (6) is also TVD from the time t_n to $t_n + \Delta t_n$, for any $\Delta t_n \leq \frac{\Delta\tau_n \Delta x^2}{\Delta x^2 + 2a_n \Delta\tau_n}$, where

$$a_n = \sup \{ a(U_{i+1}^n, x_{i+1}, t_n), a(U_{i+1/2}^n, x_{i+1/2}, t_n) : i = 0, \pm 1, \pm 2, \dots \}.$$

Proof. Note that the first equation of (6) can be written as

$$\begin{aligned}
 U_i^{n+1} = & \theta \left\{ \frac{1}{\Delta x} \int_{x_{i-1/2}}^{x_{i+1/2}} v^n(x) dx - \frac{\Delta \tau_n}{\Delta x} [f(v^n(x_{i+1/2})) - f(v^n(x_{i-1/2}))] \right\} \\
 & + \left(1 - \theta - \frac{(a(U_{i+1/2}^n, x_{i+1/2}, t_n) + a(U_{i-1/2}^n, x_{i-1/2}, t_n))\Delta t_n)}{\Delta x^2} \right) U_i^n + \frac{\Delta t_n a(U_{i-1/2}^n, x_{i-1/2}, t_n)}{\Delta x^2} U_{i-1}^n \\
 & + \frac{\Delta t_n a(U_{i+1/2}^n, x_{i+1/2}, t_n)}{\Delta x^2} U_{i+1}^n.
 \end{aligned}$$

The condition of the theorem ensures that the coefficient of U_i^n is non-negative. Therefore U_i^{n+1} in the first equation of (6) is a convex combination of $U_i^n, U_{i-1}^n, U_{i+1}^n$ and U_i^{n+1} computed from scheme (2) with the time step size $\Delta \tau_n$. Since scheme (2) is TVD for the time step size $\Delta \tau_n$, U_i^{n+1} computed by scheme (6) satisfies

$$\text{TV}\{U_i^{n+1}\} \leq \max\{\text{TV}\{U_i^n\}, \text{TV}\{U_{i+1/2}^n\}\} < \infty.$$

Similarly for the second equation of (6), the proof is complete. \square

Remark. The examples reported in the paper are aimed to show the flexibility of the new approach, and its capability to handle small time steps, without introducing excessive numerical dissipation. The more efficient way to overcome the small time step restriction is to use the implicit-explicit time discretization, e.g. [3,15,23], which treats the advection part explicitly, and the diffusion part implicitly, thus avoiding the $O(\Delta x^2)$ stability restriction on the time step due to the diffusion term, or to use a fast explicit Runge–Kutta solver, e.g. [24,30]. Well-balanced central schemes for shallow water equation have been developed both for staggered [36] and non-staggered [17] methods. Up to now the non-staggered version of the well-balanced scheme is simpler since the semi-discrete schemes maintain the numerical solution of $\frac{\partial u}{\partial t} = 0$, while staggered methods allow it only if $u = \text{constant}$. It will be interesting to see what happens when one applies the methods developed here to the balance law. These will be further explored in the future.

4. Reconstructions in one space dimension

In order to separate the two classes of cells, denote $V_i^n = U_{i+1/2}^n$ on cell $D_i = (x_i, x_{i+1})$ and denote $C_i = (x_{i-1/2}, x_{i+1/2})$, see Fig. 4. A straightforward reconstruction is to do it for the cell classes $\{C_i\}$ and $\{D_i\}$ separately. Since there is no overlapping in $\{C_i\}$ or in $\{D_i\}$, standard reconstruction methods, e.g.

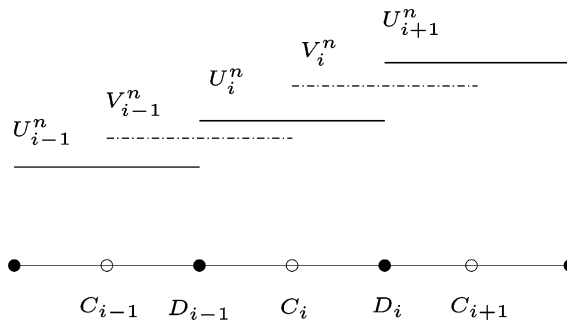


Fig. 4. 1D overlapping cells with the change of notation.

MUSCL, ENO, etc., can be applied. The interesting question is what happens if we combine the cells $\{C_i\}$ and $\{D_i\}$ in the reconstruction.

Remark. In general, since the reconstruction at each time involves two classes of cells, the complexity of a central scheme on overlapping cells is twice as much as the NT scheme or other central schemes on the staggered grid with the same order of accuracy.

4.1. A fifth order reconstruction using combined cells

Let's consider for example the reconstruction for cell C_i with the cell average U_i^n . For simplicity we only use the information from overlapping cells adjacent to cell C_i , see Fig. 4. Adapting the strategy of Abgrall [4] to overlapping cells, the highest order polynomial determined by the cell averages is fourth order. Let

$$p_4(x) = a_0 + a_1(x - x_i) + a_2(x - x_i)^2 + a_3(x - x_i)^3 + a_4(x - x_i)^4,$$

satisfy $\frac{1}{\Delta x} \int_{C_j} p_4(x) dx = U_j^n, j = i, i \pm 1$ and $\frac{1}{\Delta x} \int_{D_j} p_4(x) dx = V_j^n, j = i, i - 1$. The coefficients of p_4 are uniquely determined as follows:

$$\begin{aligned} a_0 &= [U_{i-1}^n + U_{i+1}^n + 46U_i^n - 9(V_{i-1}^n + V_i^n)]/30, \\ a_1 &= [U_{i-1}^n - U_{i+1}^n - 5(V_{i-1}^n - V_i^n)]/(3\Delta x), \\ a_2 &= -[U_{i-1}^n + U_{i+1}^n + 14U_i^n - 8(V_{i-1}^n + V_i^n)]/(2\Delta x^2), \\ a_3 &= -2[U_{i-1}^n - U_{i+1}^n - 2(V_{i-1}^n - V_i^n)]/(3\Delta x^3), \\ a_4 &= 2[U_{i-1}^n + U_{i+1}^n + 6U_i^n - 4(V_{i-1}^n + V_i^n)]/(3\Delta x^4). \end{aligned} \tag{7}$$

This reconstruction is oscillatory if the solution is non-smooth. The simplest way to overcome this problem is to combine it with lower order polynomials, using proper smoothness indicators to turn on the high order polynomial in the smooth region and turn it off in the non-smooth region. This follows the WENO strategy of Liu et al. [29], Jiang and Shu [12], Liu and Osher [28], Liu and Tadmor [31], etc. In particular, it follows [26,16] in which the reconstruction is based on the convex combination of linear polynomials and a quadratic polynomial.

Let $p_l(x)$ be the linear polynomial with the given cell averages in cells D_{i-1} and C_i and $p_r(x)$ be the linear polynomial with the given cell averages in cells C_i and D_i . Let $p(x) = w_4 p_4(x) + w_l p_l(x) + w_r p_r(x)$ where w_4, w_l, w_r are some non-negative weights satisfying $w_4 + w_l + w_r = 1$, so that $p(x)$ also has the given cell average U_i^n in cell C_i . In order to determine the weights, let IS_4, IS_l and IS_r be the corresponding smoothness indicators so that $IS_4 = 1/[(\Delta x a_4)^2 + \epsilon]$, $IS_l = 1/[IS_4 + (\Delta x p_l')^2 + \epsilon]$ and $IS_r = 1/[IS_4 + (\Delta x p_r')^2 + \epsilon]$, where $\epsilon = 10^{-6}$. Let $w = IS_4 + IS_l + IS_r$, $w_4 = IS_4/w$, $w_l = IS_l/w$ and $w_r = IS_r/w$. It is easy to see that when the stencil of cells $\{C_{i-1}, \dots, C_{i+1}\}$ contains a discontinuity of the solution, $IS_4 = O(\Delta x^6)$, and $1/IS_l, 1/IS_r = O(1)$. Therefore $w_4 = O(\Delta x^6)$ which is within the accuracy level $O(\Delta x^5)$ and it is small enough to control $p_4(x)$. Also w_l and w_r will shift the weights to the flatter linear polynomial. When the stencil lies in a smooth region of the solution, $IS_4 = O(\Delta x^{-2})$, $IS_l, IS_r = O(\Delta x^2)$, thus $w_l, w_r = O(\Delta x^4)$. Therefore w_l and w_r are small enough to scale the approximation errors of p_l and p_r down to the accuracy level $O(\Delta x^5)$. These weights satisfy the WENO principle defined in [29] and the reconstruction has fifth formal order of accuracy for smooth solutions.

4.2. A third order ENO reconstruction using combined cells

In order to construct a quadratic polynomial

$$p_2(x) = a_0 + a_1(x - x_i) + a_2(x - x_i)^2$$

in cell C_i , there are three possible ENO stencils of overlapping cells to choose from, namely $\{C_{i-1}, D_{i-1}, C_i\}$, $\{D_{i-1}, C_i, D_i\}$ or $\{C_i, D_i, C_{i+1}\}$, see Fig. 4. Viewing the cell averages as point values at their respective cell centers, the Newton divided difference [10] can be used as the smoothness indicator to pick one stencil which contains the smoothest data. For example, if the stencil $\{D_{i-1}, C_i, D_i\}$ is chosen, then the coefficients of p_2 can be determined by letting $\frac{1}{\Delta x} \int_{D_{i-1}} p_2(x) dx = V_{i-1}^n$, $\frac{1}{\Delta x} \int_{C_i} p_2(x) dx = U_i^n$ and $\frac{1}{\Delta x} \int_{D_i} p_2(x) dx = V_i^n$. The quadratic ENO reconstruction using combined overlapping cells has third formal order of accuracy for smooth solutions.

4.3. Second order ENO and MUSCL reconstructions using combined cells

We apply the second order ENO or MUSCL reconstruction for cell C_i using only the closest overlapping cells, D_{i-1} and D_i , see Fig. 4. Since the linear polynomial $p_1(x) = U_i^n + a_1(x - x_i)$ has the given cell average U_i^n in cell C_i , the only thing left is to determine the slope a_1 . The MUSCL reconstruction with the minmod function gives

$$a_1 = \text{minmod} \left\{ \frac{V_i^n - U_i^n}{\Delta x/2}, \frac{U_i^n - V_{i-1}^n}{\Delta x/2} \right\},$$

where $\text{minmod}(a, b) = \frac{1}{2} [\text{sgn}(a) + \text{sgn}(b)] \min\{|a|, |b|\}$. The ENO reconstruction gives $a_1 = \frac{V_i^n - U_i^n}{\Delta x/2}$ if $|V_i^n - U_i^n| \leq |U_i^n - V_{i-1}^n|$; $\frac{U_i^n - V_{i-1}^n}{\Delta x/2}$ otherwise. These reconstructions have second formal order of accuracy for smooth solutions.

Remark. With the MUSCL reconstruction using combined overlapping cells in 1D, and if the fluxes in scheme (2) are evaluated at the middle time level $t_n + \frac{1}{2} \Delta t_n$, then it becomes the scheme ORD in [32] with mesh size $\frac{1}{2} \Delta x$.

5. Extension to two space dimensions

Consider the conservation law in two space dimensions

$$\frac{\partial u}{\partial t} + \frac{\partial f(u)}{\partial x} + \frac{\partial g(u)}{\partial y} = 0, \quad (x, y, t) \in R^2 \times (0, T). \tag{8}$$

Assume a uniform rectangular mesh with mesh size $\Delta x \times \Delta y$ and cell center positions $\mathbf{x}_{i,j} = (x_i, y_j) = (i\Delta x, j\Delta y)$. Let $U_{i,j}^n$ approximate the cell average of u in the cell centered at $\mathbf{x}_{i,j}$ at the time t_n . The most common staggered mesh would be to shift the original mesh along the vector $(\frac{1}{2}\Delta x, \frac{1}{2}\Delta y)$, causing the cell centered at $\mathbf{x}_{i,j}$ to be shifted to a new cell centered at $\mathbf{y}_{i,j} = \mathbf{x}_{i,j} + (\frac{1}{2}\Delta x, \frac{1}{2}\Delta y)$. Let $V_{i,j}^n$ approximate the cell average of u in this the new cell at the time t_n . We have defined the approximated cell averages of u on overlapping cells (see Fig. 5, the original cells are bounded by solid lines and the shifted dual cells are bounded by dashed lines). To simplify the terminology, we call the original cell centered at $\mathbf{x}_{i,j}$ the cell of $U_{i,j}$ and the shifted dual cell centered at $\mathbf{y}_{i,j}$ the cell of $V_{i,j}$. Let $\mu^n(x, y)$ be a piecewise polynomial reconstructed on the original cells of $\{U_{i,j}\}$ and $v^n(x, y)$ be another piecewise polynomial reconstructed on the shifted dual cells of $\{V_{i,j}\}$, such that

$$\frac{1}{|\text{cell of } U_{i,j}|} \int_{\text{cell of } U_{i,j}} \mu^n(x, y) dx dy = U_{i,j}^n,$$

$$\frac{1}{|\text{cell of } V_{i,j}|} \int_{\text{cell of } V_{i,j}} v^n(x, y) dx dy = V_{i,j}^n,$$

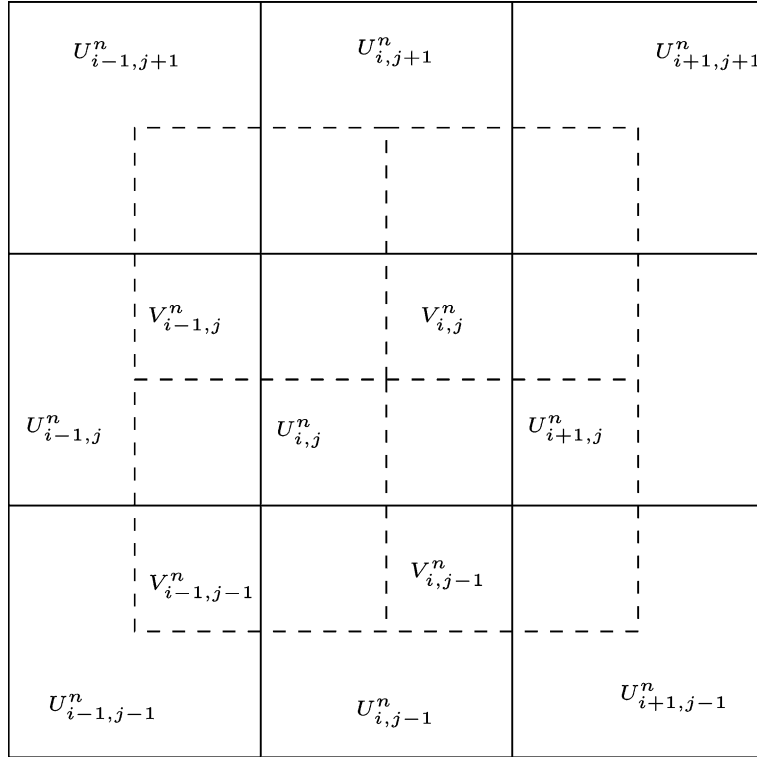


Fig. 5. 2D (staggered) overlapping cells.

where $|\text{cell of } U_{i,j}| = \Delta x \Delta y$ is the area of the cell. The 2D central scheme in the forward Euler form analogous to (3) can be written as follows:

$$\begin{aligned}
 U_{i,j}^{n+1} &= \theta \left(\frac{1}{|\text{cell of } U_{i,j}|} \int_{\text{cell of } U_{i,j}} v^n \, dx \, dy \right) \\
 &\quad + (1 - \theta) U_{i,j}^n - \frac{\Delta t_n}{|\text{cell of } U_{i,j}|} \int_{\partial(\text{cell of } U_{i,j})} (f(v^n), g(v^n)) \cdot \mathbf{n} \, ds, \\
 V_{i,j}^{n+1} &= \theta \left(\frac{1}{|\text{cell of } V_{i,j}|} \int_{\text{cell of } V_{i,j}} \mu^n \, dx \, dy \right) \\
 &\quad + (1 - \theta) V_{i,j}^n - \frac{\Delta t_n}{|\text{cell of } V_{i,j}|} \int_{\partial(\text{cell of } V_{i,j})} (f(\mu^n), g(\mu^n)) \cdot \mathbf{n} \, ds,
 \end{aligned} \tag{9}$$

where \mathbf{n} denotes unit outer normal of the corresponding cell boundary, $\theta = \Delta t_n / \Delta \tau_n \leq 1$, $\Delta t_n = t_{n+1} - t_n$ is the actual time step size, $\Delta \tau_n$ is the maximum time step size determined by the CFL restriction. The evaluation of the fluxes integrated along the cell boundary can be computed with the quadrature, see, e.g., [27]. The semi-discrete form can also be obtained as follows by moving $U_{i,j}^n$ and $V_{i,j}^n$ to the left-hand side and multiplying both sides by $\frac{1}{\Delta t_n}$, then passing to the limit as $\Delta t_n \rightarrow 0$,

$$\begin{aligned}
\frac{d}{dt} U_{i,j}(t_n) &= \frac{1}{\Delta\tau_n} \left(\frac{1}{|\text{cell of } U_{i,j}|} \int_{\text{cell of } U_{i,j}} v^n \, dx \, dy - U_{i,j}^n \right) \\
&\quad - \frac{1}{|\text{cell of } U_{i,j}|} \int_{\partial(\text{cell of } U_{i,j})} (f(v^n), g(v^n)) \cdot \mathbf{n} \, ds, \\
\frac{d}{dt} V_{i,j}(t_n) &= \frac{1}{\Delta\tau_n} \left(\frac{1}{|\text{cell of } V_{i,j}|} \int_{\text{cell of } V_{i,j}} \mu^n \, dx \, dy - V_{i,j}^n \right) \\
&\quad - \frac{1}{|\text{cell of } V_{i,j}|} \int_{\partial(\text{cell of } V_{i,j})} (f(\mu^n), g(\mu^n)) \cdot \mathbf{n} \, ds.
\end{aligned} \tag{10}$$

The TVD Runge–Kutta methods [39] or other ODE solvers can be applied to (10) to obtain a fully discrete scheme with suitable order of accuracy in time.

Remark. 1. Scheme (10) could also be adapted to a Voronoi type mesh (a triangular mesh plus its dual), so that the cells of $\{U_{i,j}\}$ represent the triangular cells and the cells of $\{V_{i,j}\}$ represent the dual cells. See [1,2] for a discussion of central finite volume schemes on unstructured meshes.

2. The central Runge–Kutta schemes [33] can also be applied to (9) so that the finite volume reconstruction is only necessary at the time t_n in order to compute the point values at cell centroids and

$$\theta \left(\frac{1}{|\text{cell of } U_{i,j}|} \int_{\text{cell of } U_{i,j}} v^n \, dx \, dy \right) + (1 - \theta) U_{i,j}^n.$$

Then reconstruction from these point values can be done at each Runge–Kutta intermediate stages to find the so called Runge–Kutta fluxes. This is more efficient in higher order case since in general, the reconstruction from point values is of lower cost than the finite volume reconstruction. This will be further explored in the future.

As in the 1D case, the reconstruction can be done for each class of cells separately or for combined overlapping cells. The second order reconstructions for combined overlapping cells are particularly simple. For example, consider the second order ENO reconstruction for the cell of $U_{i,j}^n$. Since the linear polynomial

$$p_1(\mathbf{x}) = U_{i,j}^n + \mathbf{a}_1 \cdot (\mathbf{x} - \mathbf{x}_{i,j}),$$

has the given cell average in the cell of $U_{i,j}$, where $\mathbf{x} = (x, y)$, the only thing left is to determine the gradient \mathbf{a}_1 . Note that the cell average of a function is a second order approximation to the function value at the cell centroid. These approximated function values at $\mathbf{x}_{i,j}$ and 2 nearby cell centroids determine the discrete gradient of the function at $\mathbf{x}_{i,j}$. Among all possible first order approximations of the gradient obtained by two cells and the cell of $U_{i,j}$, one can construct a discrete gradient \mathbf{a}_1 so that each of its two components is the smallest (in absolute value). In particular, the two cells can be chosen from the cells of $V_{i-1,j}$, $V_{i,j}$, $V_{i,j-1}$ or $V_{i-1,j-1}$, or from the cells of $U_{i-1,j}$, $V_{i-1,j}$, $U_{i,j+1}$, $V_{i,j}$, $U_{i+1,j}$, $V_{i,j-1}$, $U_{i,j-1}$ or $V_{i-1,j-1}$, see Fig. 5.

5.1. A third order finite volume ENO reconstruction in 2D using combined cells

Standard finite volume ENO reconstruction in 2D can be adapted to overlapping cells, see [10,38] for ENO, [27] for a finite volume WENO reconstruction for central schemes. We assume a uniform rectangular mesh with $\Delta x = \Delta y$. A typical ENO stencil with 9 combined overlapping cells E_1, E_2, \dots, E_9 is shown in Fig. 6. This stencil uniquely determines a bi-quadratic polynomial

$$P(x, y) = a_1 + a_2x + a_3y + a_4x^2 + a_5xy + a_6y^2 + a_7x^2y + a_8xy^2 + a_9x^2y^2$$

by letting $(1/|E_k|) \int_{E_k} P \, dx \, dy = U_{E_k}^n$, $k = 1, 2, \dots, 9$, where $|E_k| = \Delta x^2$ is the area of the cell and $U_{E_k}^n$ is the given cell average at cell E_k . In the following computations, the inverse of the coefficient matrix of this linear system is first found numerically and then used for all the reconstructions. There are 9 such stencils containing the cell of $U_{i,j}$ in Fig. 5, which determine 9 bi-quadratic polynomials $P_k(x, y)$, $k = 1, 2, \dots, 9$, defined on the cell of $U_{i,j}$. Among them, only one $P_k(x, y)$ will be chosen whose smoothness indicator IS_k is the smallest, where IS_k is defined as follows:

$$IS_k = |P_k(\mathbf{x}_{i,j}) - U_{i,j}^n| + \frac{\Delta x}{2} \left\{ \left| \frac{\partial P_k}{\partial x}(\mathbf{x}_{i,j}) \right| + \left| \frac{\partial P_k}{\partial y}(\mathbf{x}_{i,j}) \right| \right\} + \frac{\Delta x^2}{3} \left\{ \left| \frac{\partial^2 P_k}{\partial x^2}(\mathbf{x}_{i,j}) \right| + \left| \frac{\partial^2 P_k}{\partial x \partial y}(\mathbf{x}_{i,j}) \right| + \left| \frac{\partial^2 P_k}{\partial y^2}(\mathbf{x}_{i,j}) \right| \right\}.$$

The chosen $P_i(x, y)$ defined on the cell of $U_{i,j}$ will be the reconstructed polynomial on the cell of $U_{i,j}$. This should be done for all the cells of $\{U_{i,j}\}$ in order to obtain the piecewise polynomial $\mu(x, y)$, similarly for the reconstruction of the piecewise polynomial $v(x, y)$ for the cells of $\{V_{i,j}\}$.

6. Numerical experiments

Scheme (4) with the r th order ($r = 2, 3$) ENO reconstruction which is separate for the two classes of cells is referred to as CO-ENO- r and has r th formal order of accuracy for smooth solutions. If the reconstruction is done by combining the overlapping cells, it is referred to as COC-ENO- r (r th order). Scheme (4) with the reconstruction presented in Section 4.1 is referred to as COC-WENO-2-5. Scheme (10) with the third order ENO reconstruction presented in Section 5.1 is still referred to as COC-ENO-3. The corresponding (up to third order) TVD Runge–Kutta time discretization methods are applied to the above schemes. Only the solution in one class of the overlapping cells is shown in the graphs throughout this section. The second order scheme developed in [18] is referred to as FD2. For systems of equations, the component-wise extensions of the scalar schemes (without characteristic decomposition) have been used in all the computations.

Example 1. We test the convergence of several schemes for the 1D linear advection equation

$$u_t + u_x = 0, \quad x \in [0, 2]; \quad u(x, 0) = 1 + \sin(\pi x), \quad x \in [0, 2],$$

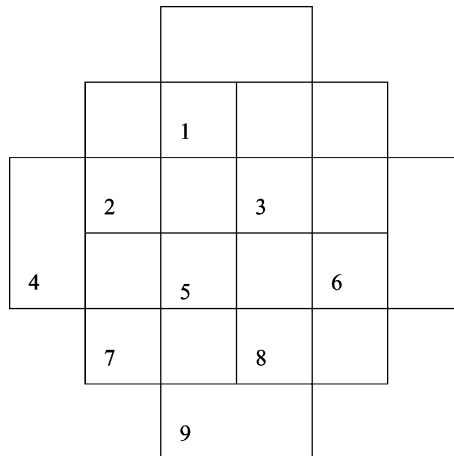


Fig. 6. ENO stencil with combined overlapping cells.

with periodic boundary conditions. The final time is $T = 2$. For the central schemes on overlapping cells, $\Delta\tau_n$ is chosen with CFL factor 0.45, $\Delta t_n = 0.5\Delta\tau_n$. For the NT scheme, Δt_n is determined with CFL factor 0.45 (see Tables 1–6). The relative l_1 and l_∞ errors are defined as $\|u - U\|_1 = \sum_i |u_i - U_i| \Delta x / \sum_i |u_i| \Delta x$ and $\|u - U\|_\infty = \max_i |u_i - U_i| / \max_i |u_i|$ respectively. It seems that the error when applying reconstruction for combined overlapping cells is about $1/r$ times the error when applying reconstruction for two classes of cells separately, where r is the order of the scheme (see e_2/e_1 and E_2/E_1 in Table 3, e_4/e_3 and E_4/E_3 in Table 5). This is clearly related to the smaller distance between the two overlapping cell centers. The slight degeneration of accuracy with the second order ENO reconstruction is related to the non-smoothness of the numerical flux caused by the abrupt shifting of the stencil. This problem can be fixed. See [37,35] for a discussion of this problem and [6] for a central scheme setting. The smaller errors of

Table 1
NT scheme

Δx	1/20	1/40	1/80	1/160	1/320
Rel. l_1 error	0.00545	0.00148	0.000392	0.000104	2.69e-05
Order	–	1.88	1.92	1.97	1.89
Rel. l_∞ error	0.0110	0.00460	0.00189	0.000774	0.000314
Order	–	1.26	1.28	1.29	1.30

Table 2
COC-ENO-2

Δx	1/20	1/40	1/80	1/160	1/320
Rel. l_1 error e_1	0.0145	0.00400	0.00108	0.000291	7.65e-05
Order	–	1.86	1.89	1.89	1.93
Rel. l_∞ error E_1	0.0219	0.00920	0.00378	0.00153	0.000618
Order	–	1.25	1.28	1.30	1.31
Rel. l_1 error e_1^*	0.00300	0.000775	0.000206	5.35e-05	1.39e-05

Table 3
CO-ENO-2

Δx	1/20	1/40	1/80	1/160	1/320
Rel. l_1 error e_2	0.0272	0.00767	0.00208	0.000568	0.000150
e_2/e_1	1.88	1.92	1.93	1.95	1.96
Rel. l_∞ error E_2	0.0353	0.0148	0.00609	0.00247	0.000997
E_2/E_1	1.61	1.61	1.61	1.61	1.61

Table 4
COC-ENO-3

Δx	1/20	1/40	1/80	1/160	1/320
Rel. l_1 error e_3	0.000277	3.46e-05	4.32e-06	5.40e-07	6.75e-08
Order	–	3.00	3.00	3.00	3.00
Rel. l_∞ error E_3	0.000223	2.77e-05	3.45e-06	4.31e-07	5.37e-08
Order	–	3.01	3.01	3.00	3.00

Table 5
CO-ENO-3

Δx	1/20	1/40	1/80	1/160	1/320
Rel. l_1 error e_4	0.000816	0.000102	1.27e-05	1.59e-06	1.99e-07
e_4/e_3	2.95	2.95	2.94	2.94	2.95
Rel. l_∞ error E_4	0.000683	8.47e-05	1.06e-05	1.31e-06	1.62e-07
E_4/E_3	3.06	3.06	3.07	3.04	3.02

Table 6
COC-WENO-2-5, $\Delta t_n = \min\{\frac{1}{2}\Delta\tau_n, \Delta x^{5/3}\}$

Δx	1/20	1/40	1/80	1/160	1/320
Rel. l_1 error	1.39e-05	2.26e-07	3.76e-09	7.25e-11	2.18e-12
Order	–	5.94	5.91	5.70	5.06
Rel. l_∞ error	1.76e-05	3.06e-07	5.48e-09	1.09e-10	2.20e-12
Order	–	5.85	5.80	5.65	5.63

the NT scheme are due to its predictor-corrector time discretization. To see this, we compute e_1^* in Table 2 using COC-ENO-2 ($\Delta t_n = 0.44\Delta x$, $\Delta\tau_n = 0.45\Delta x$) with the fluxes in (3) evaluated at $t_n + \frac{1}{2}\Delta t_n$. The resulting errors are about half of the sizes of the corresponding l_1 errors in Table 1.

Example 2. We test the numerical dissipation of scheme CO-ENO-2 for the 1D Burgers equation

$$u_t + \left(\frac{1}{2}u^2\right)_x = 0, \quad x \in [0, 2]; \quad u(x, 0) = 1 + \sin(\pi x), \quad x \in [0, 2],$$

with periodic boundary conditions. The final time is $T = 0.7$. In Fig. 7(a) and (b), we fix $\Delta\tau_n = \Delta x/4$ and choose the time step sizes $\Delta t_n = \Delta x/4$ and $(\Delta x/4)^2$ respectively. There is no significant difference between the two results. As a comparison, in Fig. 7(c), we compute the same problem again with $\Delta\tau_n = \Delta t_n = (\Delta x/4)^2$. It is clear that the numerical dissipation increases as $\Delta\tau_n \rightarrow 0$.

Example 3. We compute a hyperbolic–parabolic equation [18] using scheme (6) with the quadratic ENO reconstruction for combined overlapping cells (Section 4.2). Eq. (5) is set with $f(u) = u^2$, $a(u, x, t) = 0$ if $|u| \leq 0.25$; $a(u, x, t) = 0.1$ if $|u| > 0.25$. The initial value is

$$u_0(x) = \begin{cases} 1, & -\frac{1}{\sqrt{2}} - 0.4 < x < -\frac{1}{\sqrt{2}} + 0.4, \\ -1, & \frac{1}{\sqrt{2}} - 0.4 < x < \frac{1}{\sqrt{2}} + 0.4, \\ 0, & \text{otherwise.} \end{cases}$$

We take $\Delta\tau_n = 0.24\Delta x$ by the CFL restriction of the hyperbolic part of the equation. The actual time step size is $\Delta t_n = \Delta x\Delta\tau_n$. The results are shown in Fig. 8 at $T = 0.7$. Clearly the small time step size doesn't seem to introduce excessive numerical dissipation.

Example 4. The nonlinear Buckley–Leverett problem (with a non-convex flux) is $u_t + f(u)_x = 0$, with $f(u) = 4u^2/(4u^2 + (1 - u)^2)$. Initially, $u = 1$ in $[-1/2, 0]$ and $u = 0$ elsewhere in the computational domain $[-1, 1]$. We want to see if COC-ENO-3 converges to the entropy solution. In Fig. 9, the computational results are plotted against the exact solution at $T = 0.4$, with $\Delta x = 1/40$, $\Delta\tau_n = 0.1\Delta x$, $\Delta t_n = 0.5\Delta\tau_n$ on the left, $\Delta t_n = 0.01\Delta\tau_n$ on the right. There seems to be no significant difference between them.

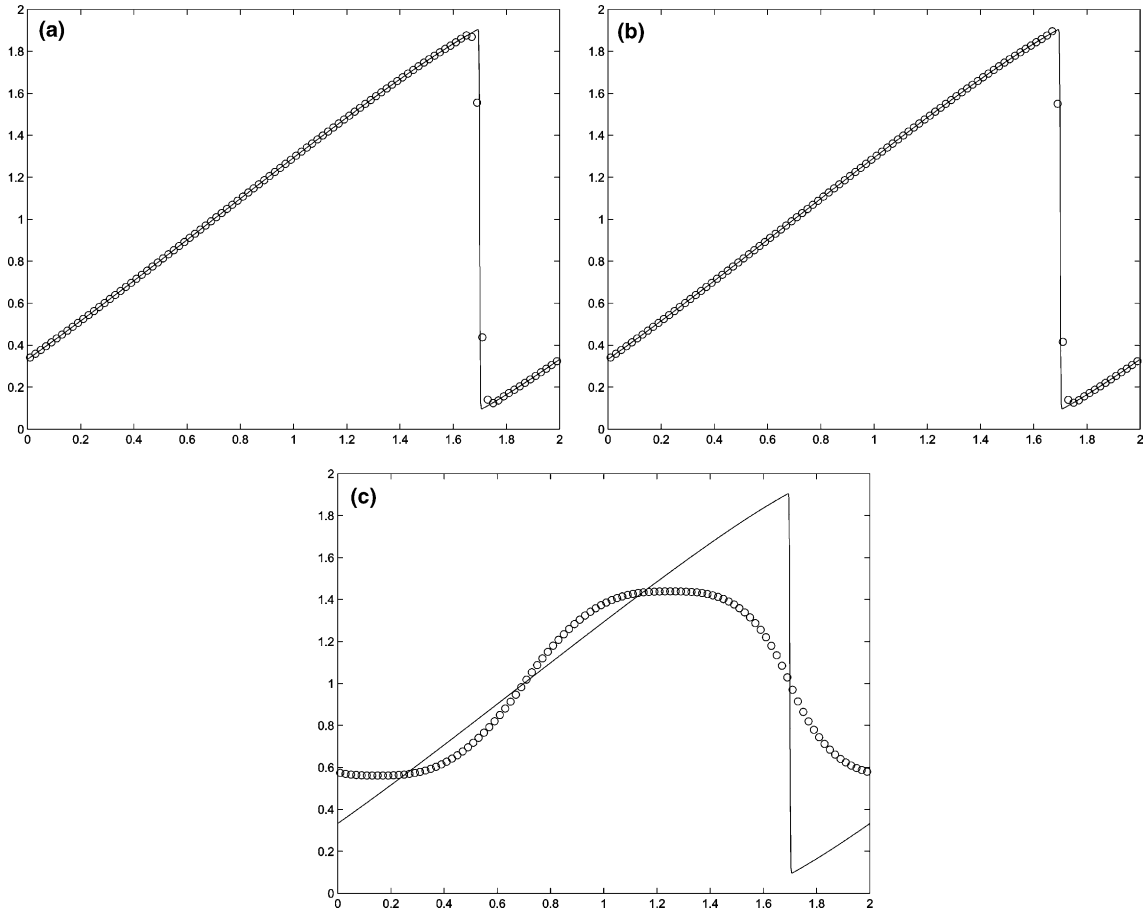


Fig. 7. Comparative results for Burgers equation by CO-ENO-2, $\Delta x = 0.02$, $T = 0.7$. (a) $\Delta\tau_n = \frac{1}{4}\Delta x$, $\Delta t_n = \frac{1}{4}\Delta x$. (b) $\Delta\tau_n = \frac{1}{4}\Delta x$, $\Delta t_n = (\frac{1}{4}\Delta x)^2$. (c) $\Delta\tau_n = \Delta t_n = (\frac{1}{4}\Delta x)^2$.

Example 5. We compute the Euler equation with Lax's initial data. $u_t + f(u)_x = 0$ with $u = (\rho, \rho v, E)^T$, $f(u) = (\rho v, \rho v^2 + p, v(E + p))^T$, $p = (\gamma - 1)(E - \frac{1}{2}\rho v^2)$, $\gamma = 1.4$. Initially, the density ρ , momentum ρv and total energy E are 0.445, 0.311 and 8.928 in $(0, 0.5)$; 0.5, 0 and 1.4275 in $(0.5, 1)$. The computed density profiles by various numerical schemes are shown at $T = 0.16$ in Fig. 10 with $\Delta x = 1/100$ by default. For the central schemes on overlapping cells, $\Delta\tau_n$ is chosen with CFL factor 0.4, $\Delta t_n = 0.5\Delta\tau_n$. For the NT scheme and FD2, Δt_n is chosen with CFL factor 0.4 and 0.9 respectively. Fig. 10(h) is computed by COC-ENO-2 with $\Delta x \approx \sqrt{2}/100$ which has half of the complexity as in Fig. 10(g). For this mesh size the complexity (when $\Delta t_n = \Delta\tau_n$) is about the same as the NT scheme (see Fig. 10(e)), but the upper bound $\Delta\tau_n$ of the time step size is larger and the computational results remain almost the same for any $\Delta t_n \in (0, \Delta\tau_n]$ (because there is no $O(1/\Delta t)$ dependent dissipation).

Example 6. Shu–Osher problem [40]. It is the Euler equation with initial data

$$\begin{aligned}
 (\rho, v, p) &= (3.857143, 2.629369, 10.333333) \quad \text{for } x < -4, \\
 (\rho, v, p) &= (1 + 0.2 \sin(5x), 0, 1) \quad \text{for } x \geq -4.
 \end{aligned}$$

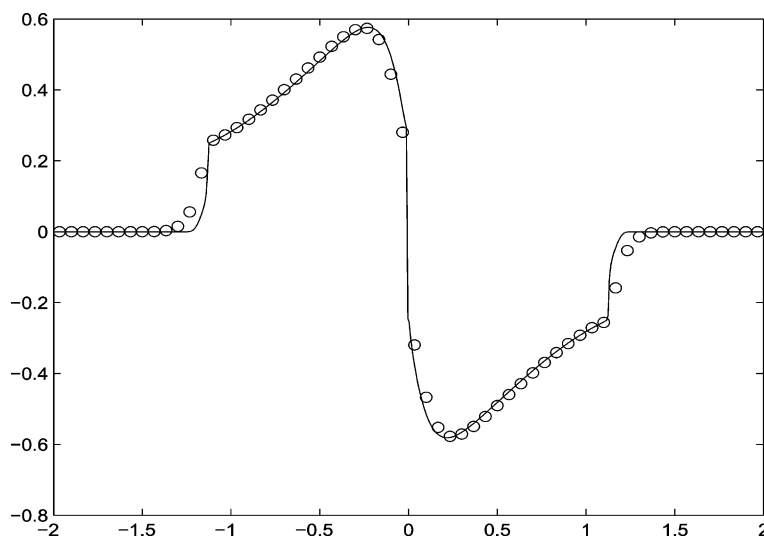


Fig. 8. Hyperbolic-parabolic problem. “o”: $\Delta x = 1/15$; “-”: $\Delta x = 1/125$.

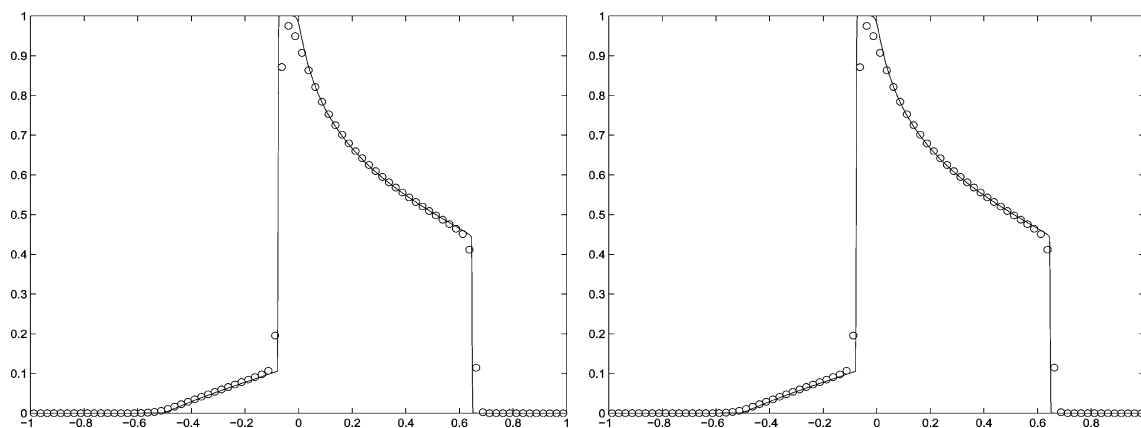


Fig. 9. Buckley–Leverett Problem computed with COC-ENO-3. $\Delta x = 1/40$, $T = 0.4$, $\Delta \tau_n = 0.1\Delta x$. Left: $\Delta t_n = 0.5\Delta \tau_n$. Right: $\Delta t_n = 0.01\Delta \tau_n$.

The density profiles are plotted at $T = 1.8$, with $\Delta x = 1/40$ by default, see Fig. 11. For the central schemes on overlapping cells, $\Delta \tau_n$ is chosen with CFL factor 0.45, $\Delta t_n = 0.5\Delta \tau_n$. For the NT scheme and FD2, Δt_n is chosen with CFL factor 0.45 and 0.9 respectively. Note that the results in Fig. 11(a) and (e) are at the same complexity level. Roughly speaking, for the same mesh size, CO-ENO- r has about the same resolution as previous staggered central schemes of similar order, while COC-ENO- r seems to provide better resolution in avoiding oscillation when using reconstructions based only on conservative variables. We have also tested COC-ENO-3 with $\Delta x \approx \sqrt{2}/40$ (so that its complexity is reduced by $\frac{1}{2}$) and found the result (not shown) very similar to the one in Fig. 11(g). The non-staggered FD2 can have twice as large time step size as the staggered schemes. When its mesh size is reduced to such that its complexity matches that of the NT scheme or COC-ENO-2, its resolution (not shown here) is slightly higher for the Lax problem but is slightly

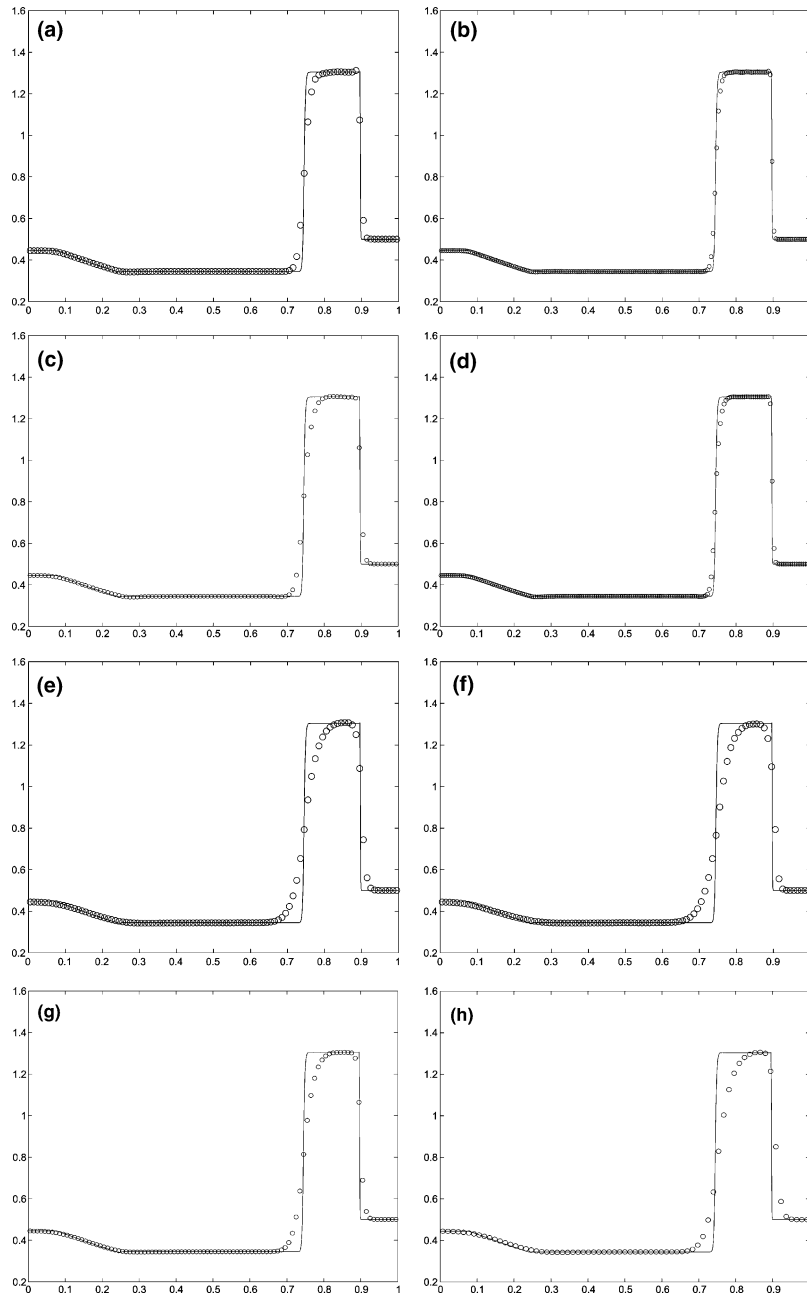


Fig. 10. Comparative results of density for Lax's Problem, $\Delta x = 1/100$ by default. (a) COC-ENO-3; (b) COC-ENO-3 ($\Delta x = 1/200$); (c) COC-WENO-2-5; (d) COC-WENO-2-5 ($\Delta x = 1/200$); (e) NT scheme; (f) FD2; (g) COC-ENO-2; (h) COC-ENO-2 ($\Delta x \approx \sqrt{2}/100$).

lower for the Shu-Osher problem than both schemes. Although the resolution of COC-WENO-2-5 is not as high as COC-ENO-3, it is much better than the other second order schemes. In 2D its cost could be much smaller than COC-ENO-3. This will be further studied in the future.

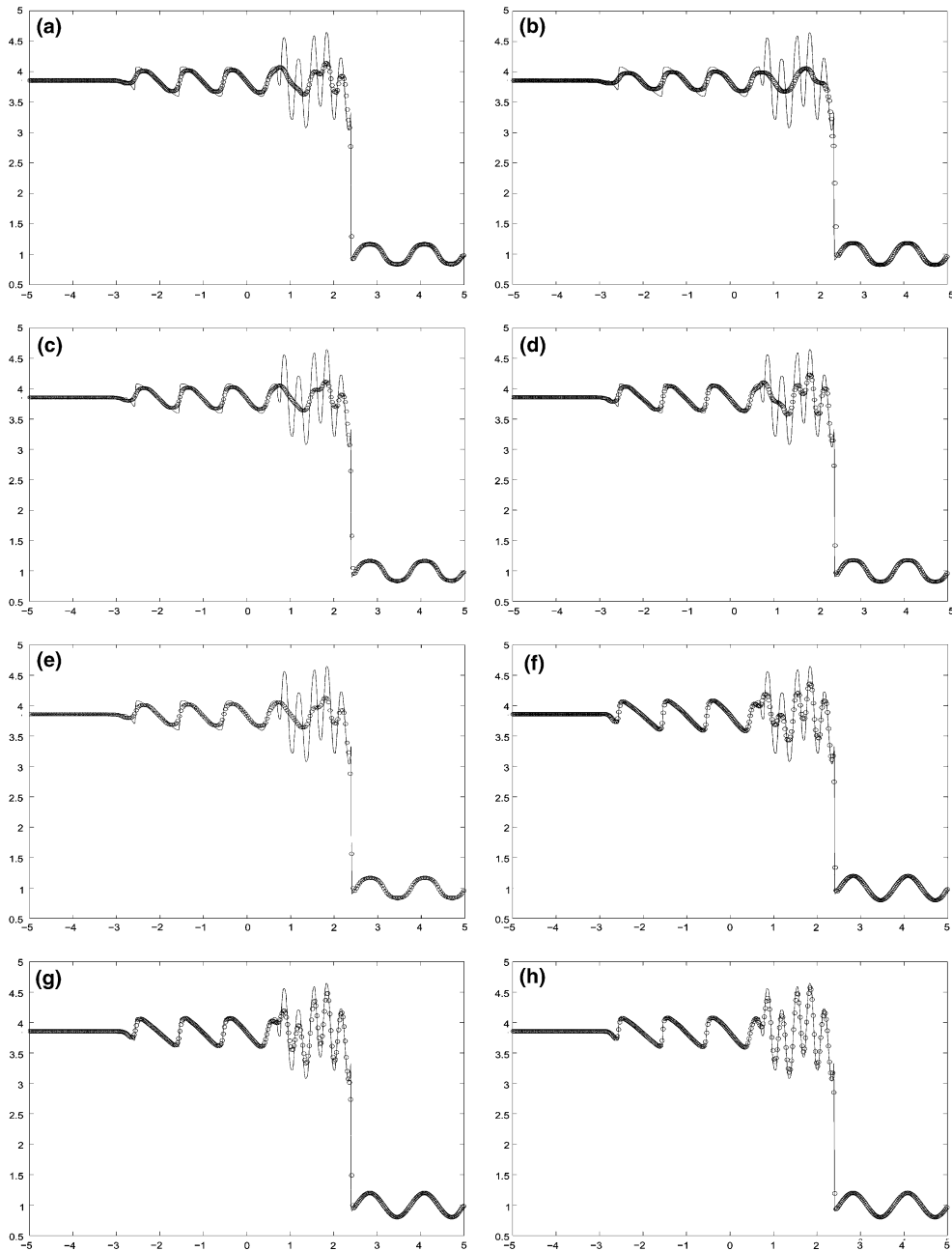


Fig. 11. Shu–Osher Problem, $\Delta x = 1/40$ by default. (a) NT scheme; (b) FD2; (c) CO-ENO-2; (d) COC-ENO-2; (e) COC-ENO-2 ($\Delta t \approx \sqrt{2}/40$); (f) COC-WENO-2-5; (g) CO-ENO-3; (h) COC-ENO-3.

Example 7. Woodward and Colella problem [43] for the Euler equation computed by COC-ENO-3. Initially, the density, momentum, total energy are 1, 0, 2500 in (0, 0.1); 1, 0, 0.025 in (0.1, 0.9); 1, 0, 250 in (0.9, 1). The density, velocity and pressure profiles are plotted in Fig. 12 ($T = 0.01$) and Fig. 13 ($T = 0.03$)

and 0.038). The density peak in Fig. 12(a) seems to be quite close to the fine solution (computed with $\Delta x = 1/2000$).

Example 8. Double Mach reflection [43] computed by COC-ENO-3. A planar Mach 10 shock is incident on an oblique wedge at a $\pi/3$ angle. The air in front of the shock has density 1.4, pressure 1 and velocity 0. The boundary condition is described in [43]. The 2D Euler equation can written as

$$\mathbf{u}_t + \mathbf{f}(\mathbf{u})_x + \mathbf{g}(\mathbf{u})_y = 0, \quad \mathbf{u} = (\rho, \rho u, \rho v, E)^T, \quad p = (\gamma - 1) \left(E - \frac{1}{2} \rho(u^2 + v^2) \right),$$

$$\mathbf{f}(\mathbf{u}) = (\rho u, \rho u^2 + p, \rho uv, u(E + p))^T, \quad \mathbf{g}(\mathbf{u}) = (\rho v, \rho uv, \rho v^2 + p, v(E + p))^T,$$

where $\gamma = 1.4$. The boundary passes through the cell edges of one class of the overlapping cells, e.g. the cells of $\{U_{i,j}\}$ in Fig. 5. The ghost cell averages (completely outside the domain) of both classes of the cells can be set according to the boundary condition. The cell averages $\{V_{i,j}^n\}$ of the cells being cut through by the

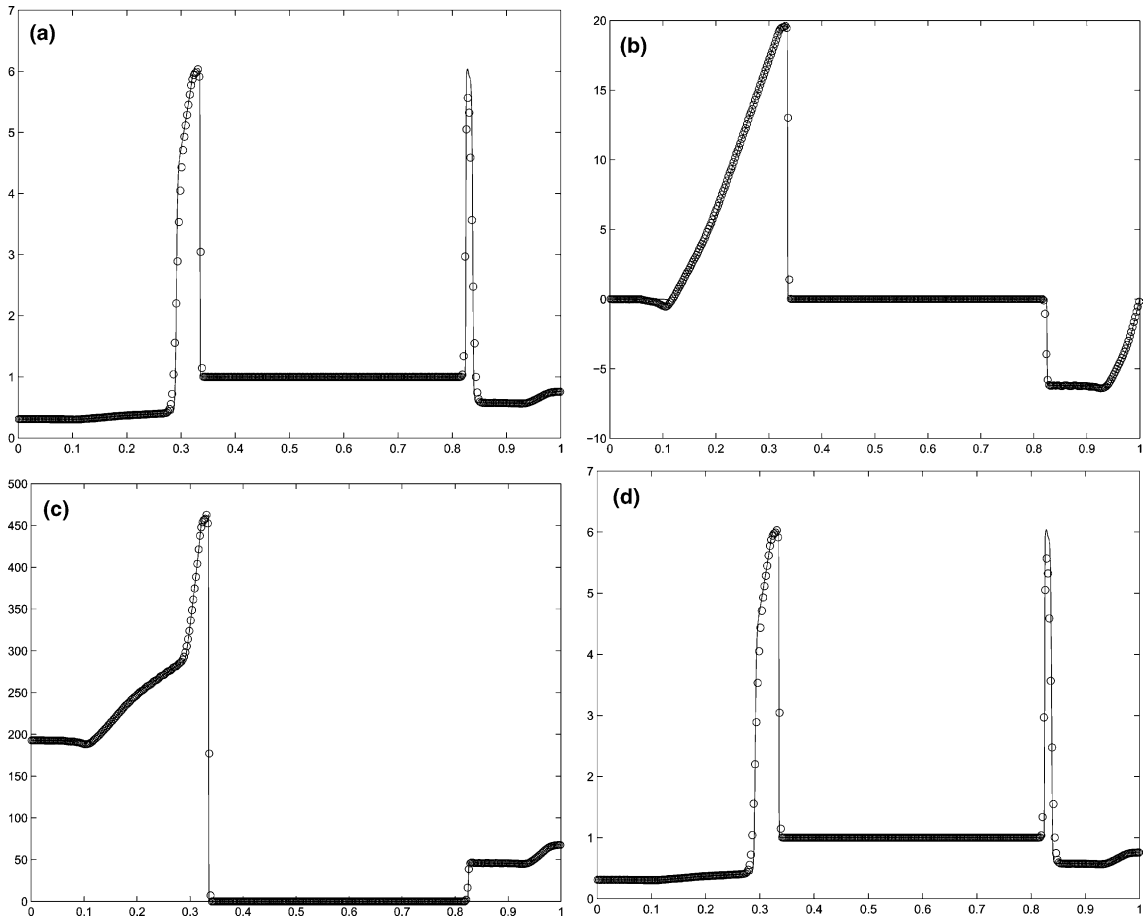


Fig. 12. Woodward and Colella Problem computed by COC-ENO-3. $\Delta x = 1/400$, $T = 0.01$, $\Delta \tau_n$ chosen with CFL factor 0.45, $\Delta t_n = \frac{1}{2} \Delta \tau_n$ by default. (a) density; (b) velocity; (c) pressure; (d) density, $\Delta t_n = 0.01 \Delta \tau_n$.

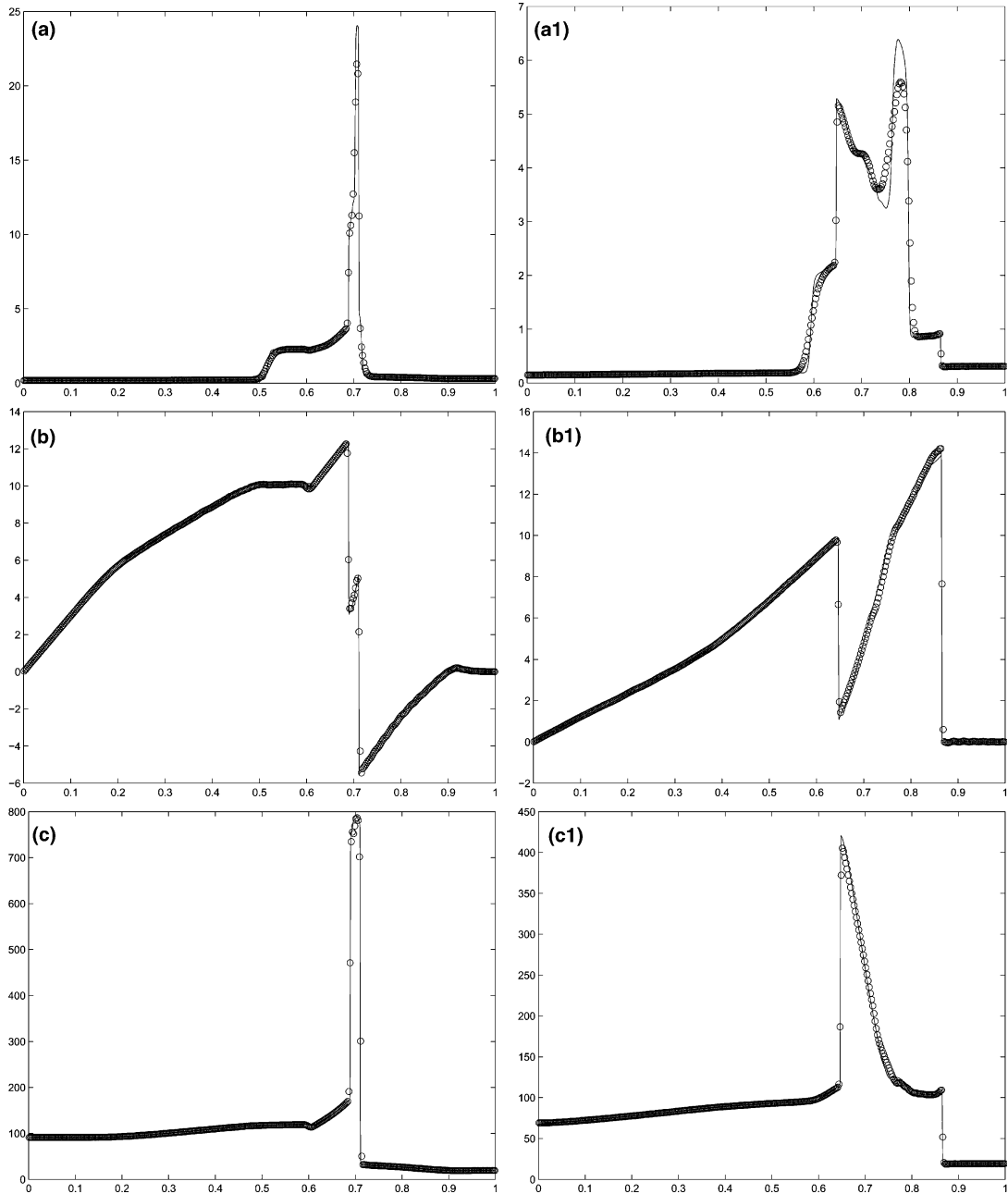


Fig. 13. Woodward and Colella Problem computed by COC-ENO-3. $\Delta x = 1/400$, $\Delta \tau_n$ chosen with CFL factor 0.45, $\Delta t_n = \frac{1}{2} \Delta \tau_n$. On the left, $T = 0.03$, (a) density; (b) velocity; (c) pressure. On the right, $T = 0.038$, (a1) density; (b1) velocity; (c1) pressure.

boundary are computed by the second equation of (10) from the cell averages at the previous time level, thus avoiding the problem of setting boundary values for them. The density and pressure profiles are plotted at $T = 0.2$ in Fig. 14, with 30 equally spaced contours.

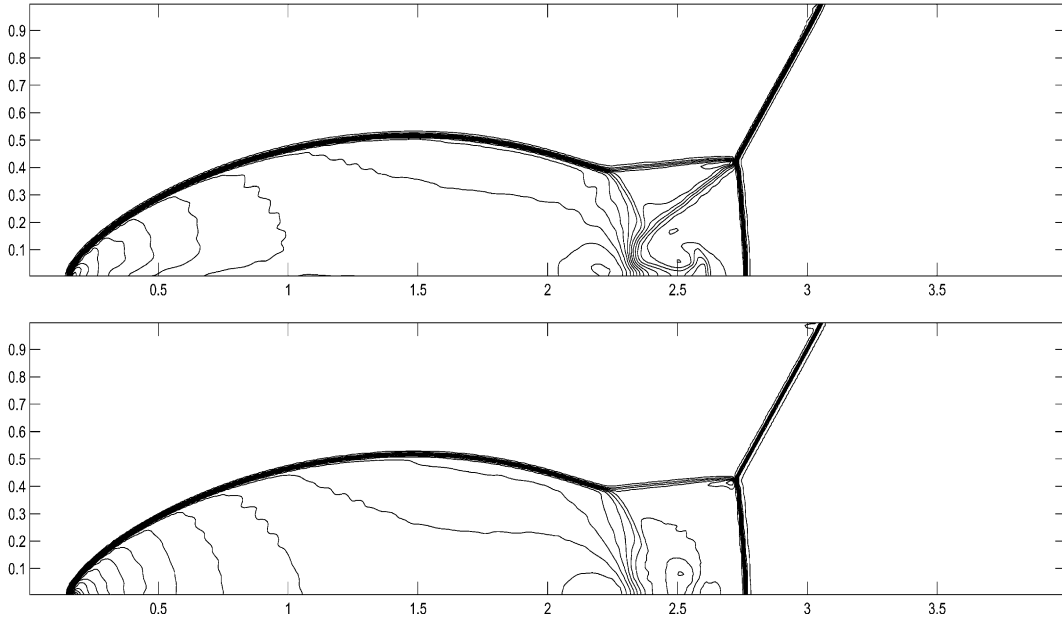


Fig. 14. Double Mach reflection computed by COC-ENO-3. $\Delta x = \Delta y = 1/120$, $\Delta \tau_n$ chosen with CFL factor 0.4, $\Delta t_n = 0.9\Delta \tau_n$. Upper: density. Lower: pressure.

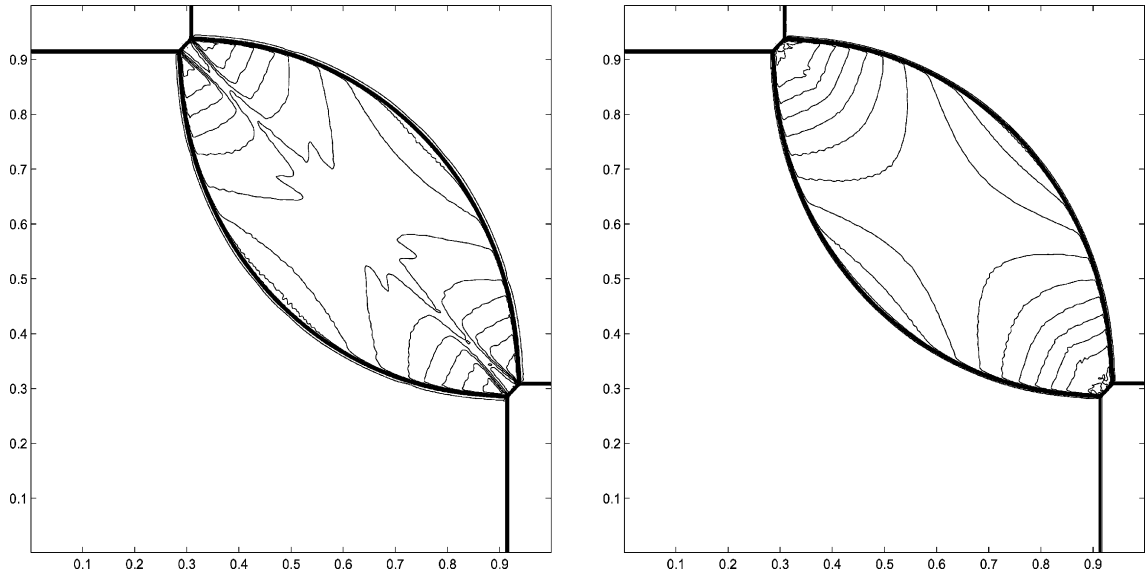


Fig. 15. 2D Riemann problem computed by COC-ENO-3. $\Delta x = \Delta y = 1/400$, $\Delta \tau_n$ chosen with CFL factor 0.4, $\Delta t_n = 0.9\Delta \tau_n$. Left: density. Right: pressure.

Example 9. 2D Riemann problem [22] for the Euler equation computed by COC-ENO-3. The computational domain is $[0,1] \times [0,1]$. The initial states are constants within each of the 4 quadrants. Counter-clock-wisely from the upper right quadrant, they are labeled as (ρ_i, u_i, v_i, p_i) , $i = 1, 2, 3, 4$. Initially, $\rho_1 = 1.1$, $u_1 = 0$, $v_1 = 0$, $p_1 = 1.1$; $\rho_2 = 0.5065$, $u_2 = 0.8939$, $v_2 = 0$, $p_2 = 0.35$; $\rho_3 = 1.1$, $u_3 = 0.8939$,

$v_3 = 0.8939$, $p_3 = 1.1$; $\rho_4 = 0.5065$, $u_4 = 0$, $v_4 = 0.8939$, $p_4 = 0.35$. The density and pressure profiles are plotted at $T = 0.25$ in Fig. 15, with 30 equally spaced contours.

Acknowledgements

I would like to thank the referees for their many useful suggestions for improving this paper, Chi-Wang Shu for a helpful discussion on the ENO smoothness indicator and Linda Heidinger for helpful editorial comments.

References

- [1] P. Arminjon, A. St-Cyr, Nessyahu–Tadmor-type central finite volume methods without predictor for 3D Cartesian and unstructured tetrahedral grids, *Appl. Numer. Math.* 46 (2) (2003) 135–155.
- [2] P. Arminjon, M.-C. Viallon, Convergence of a finite volume extension of the Nessyahu–Tadmor scheme on unstructured grids for a two-dimensional linear hyperbolic equation, *SIAM J. Numer. Anal.* 36 (1999) 738–771.
- [3] U. Ascher, S. Ruuth, R.J. Spiteri, Implicit–explicit Runge–Kutta methods for time dependent partial differential equations, *Appl. Numer. Math.* 25 (1997) 151–167.
- [4] R. Abgrall, On essentially non-oscillatory schemes on unstructured meshes: analysis and implementation, *J. Comput. Phys.* 114 (1994) 45–58.
- [5] T. Barth, P. Frederickson, High order solution of the Euler equations on unstructured grids using quadratic reconstruction, AIAA Paper No. 90-0013.
- [6] F. Bianco, G. Puppo, G. Russo, High-order central schemes for hyperbolic systems of conservation laws, *SIAM J. Sci. Comput.* 21 (1) (1999) 294–322.
- [7] S. Bryson, D. Levy, High-order central WENO schemes for multidimensional Hamilton–Jacobi equations, *SIAM J. Numer. Anal.* 41 (2003) 1339–1369.
- [8] J. Glimm, Solution in the large for nonlinear hyperbolic systems of equations, *Comm. Pure Appl. Math.* 18 (1965) 697–715.
- [10] A. Harten, B. Engquist, S. Osher, S.R. Chakravarthy, Uniformly high-order accurate essentially non-oscillatory schemes, III, *J. Comput. Phys.* 71 (2) (1987) 231–303.
- [11] G.-S. Jiang, D. Levy, C.-T. Lin, S. Osher, E. Tadmor, High-resolution non-oscillatory central schemes with non-staggered grids for hyperbolic conservation laws, *SIAM J. Numer. Anal.* 35 (1998) 2147.
- [12] G.-S. Jiang, C.-W. Shu, Efficient implementation of weighted ENO schemes, *J. Comput. Phys.* 126 (1996) 202–228.
- [13] G.-S. Jiang, E. Tadmor, Non-oscillatory central schemes for multidimensional hyperbolic conservation laws, *SIAM J. Sci. Comput.* 19 (6) (1998) 1892–1917.
- [14] S. Jin, Z. Xin, The relaxation schemes for systems of conservation laws in arbitrary space dimensions, *Comm. Pure Appl. Math.* 48 (3) (1995) 235–276.
- [15] C.A. Kennedy, M.H. Carpenter, Additive Runge–Kutta schemes for convection–diffusion–reaction equations, *Appl. Numer. Math.* 44 (2003) 139–181.
- [16] A. Kurganov, D. Levy, A third-order semi-discrete central scheme for conservation laws and convection–diffusion equations, *SIAM J. Sci. Comput.* 22 (4) (2000) 1461–1488.
- [17] A. Kurganov, D. Levy, Central-upwind schemes for the Saint-Venant system, *M2AN Math. Model. Numer. Anal.* 36 (2002) 397–425.
- [18] A. Kurganov, E. Tadmor, New high-resolution central schemes for nonlinear conservation laws and convection–diffusion equations, *J. Comput. Phys.* 160 (1) (2000) 241–282.
- [19] A. Kurganov, E. Tadmor, New high-resolution semi-discrete central schemes for Hamilton–Jacobi equations, *J. Comput. Phys.* 160 (2000) 720–742.
- [20] A. Kurganov, G. Petrova, A third-order semi-discrete genuinely multidimensional central scheme for hyperbolic conservation laws and related problems, *Numer. Math.* 88 (4) (2001) 683–729.
- [21] P.D. Lax, Weak solutions of nonlinear hyperbolic equations and their numerical computation, *Comm. Pure Appl. Math.* 7 (1954) 159–193.
- [22] P. Lax, X.-D. Liu, Solution of two dimensional Riemann problem of gas dynamics by positive schemes, *SIAM J. Sci. Comput.* 19 (2) (1998) 319–340.

- [23] S.F. Liotta, V. Romano, G. Russo, Central schemes for balance laws of relaxation type, *SIAM J. Numer. Anal.* 38 (2000) 1337–1356.
- [24] V.I. Lebedev, Explicit difference schemes for solving stiff systems of ODEs and PDEs with complex spectrum, *Russian J. Numer. Anal. Math. Modell.* 13 (1998) 107–116.
- [25] D. Levy, G. Puppo, G. Russo, Central WENO schemes for nonlinear conservation laws, *Math. Model. Numer. Anal.* 33 (1999) 547.
- [26] D. Levy, G. Puppo, G. Russo, Compact central WENO schemes for multidimensional conservation laws, *SIAM J. Sci. Comput.* 22 (2) (2000) 656–672.
- [27] D. Levy, G. Puppo, G. Russo, A fourth-order central WENO scheme for multidimensional hyperbolic systems of conservation laws, *SIAM J. Sci. Comput.* 24 (2) (2002) 480–506.
- [28] X.-D. Liu, S. Osher, Convex ENO high order multi-dimensional schemes without field by field decomposition or staggered grids, *J. Comput. Phys.* 142 (2) (1998) 304–330.
- [29] X.-D. Liu, S. Osher, T. Chan, Weighted essentially non-oscillatory schemes, *J. Comput. Phys.* 115 (1) (1994) 200–212.
- [30] A.A. Medovikov, High order explicit methods for parabolic equations, *BIT* 38 (1998) 372–390.
- [31] X.-D. Liu, E. Tadmor, Third order nonoscillatory central scheme for hyperbolic conservation laws, *Numer. Math.* 79 (3) (1998) 397–425.
- [32] H. Nessyahu, E. Tadmor, Nonoscillatory central differencing for hyperbolic conservation laws, *J. Comput. Phys.* 87 (2) (1990) 408–463.
- [33] L. Pareschi, G. Puppo, G. Russo, Central Runge–Kutta schemes for conservation laws, *SIAM J. Sci. Comput.* 26 (2005) 979–999.
- [34] J. Qiu, C.-W. Shu, On the construction, comparison, and local characteristic decomposition for high-order central WENO schemes, *J. Comput. Phys.* 183 (1) (2002) 187–209.
- [35] A.M. Rogerson, E. Meiburg, A numerical study of the convergence properties of ENO schemes, *J. Sci. Comput.* 5 (1990) 151–167.
- [36] G. Russo, Central schemes for balance laws, in: *Hyperbolic Problems: Theory, Numerics, Applications*, vols. I, II (Magdeburg, 2000), pp. 821–829, in: *Internat. Ser. Numer. Math.*, vols. 140, 141, Birkhuser, Basel.
- [37] C.-W. Shu, Numerical experiments on the accuracy of ENO and modified ENO schemes, *J. Sci. Comput.* 5 (1990) 127–149.
- [38] C.-W. Shu, Essentially non-oscillatory and weighted essentially non-oscillatory schemes for hyperbolic conservation laws, in: A. Quarteroni (Ed.), *Advanced Numerical Approximation of Nonlinear Hyperbolic Equations*, *Lecture Notes in Mathematics*, vol. 1697, Springer, Berlin, 1998.
- [39] C.-W. Shu, S. Osher, Efficient implementation of essentially non-oscillatory shock-capturing schemes, *J. Comput. Phys.* 77 (2) (1988) 439–471.
- [40] C.-W. Shu, S. Osher, Efficient implementation of essentially nonoscillatory shock-capturing schemes, II, *J. Comput. Phys.* 83 (1) (1989) 32–78.
- [41] H.-Z. Tang, T. Tang, Adaptive mesh methods for one- and two-dimensional hyperbolic conservation laws, *SIAM J. Numer. Anal.* 41 (2003) 487–515.
- [42] B. van Leer, Towards the ultimate conservative difference scheme V, A second-order sequel to Godunov’s method, *J. Comput. Phys.* 32 (1979) 101–136.
- [43] P. Woodward, P. Colella, The numerical simulation of two-dimensional fluid flow with strong shocks, *J. Comput. Phys.* 54 (1) (1984) 115–173.
- [44] M. Zennaro, Natural continuous extensions of Runge–Kutta methods, *Math. Comput.* 46 (1986) 119.